Supporting Information

Rational Design of a Self-Supporting Skeleton Decorated with Dual Lithiophilic Sn-Containing and N-Doped Carbon Tubes for Dendrite-free Lithium Metal Anode

Jiaxiao Ge,[a]† Jie Hong,[a]† Tiancun Liu[ab] and Yong Wang[ac]**

[a]*Department of Chemical Engineering, School of Environmental and Chemical Engineering, Shanghai University, 99 Shangda Road, Shanghai 200444, People's Republic of China*

[b]*School of Materials Science and Engineering, Zhejiang Sci-Tech University, Hangzhou 310018, People's Republic of China, Email address: liutc@zstu.edu.cn*

[c]*Key Laboratory of Organic Compound Pollution Control Engineering (MOE), Shanghai University, 99 Shangda Road, Shanghai 200444, People's Republic of China, Email address: yongwang@shu.edu.cn*

†These authors contributed equally to this work.

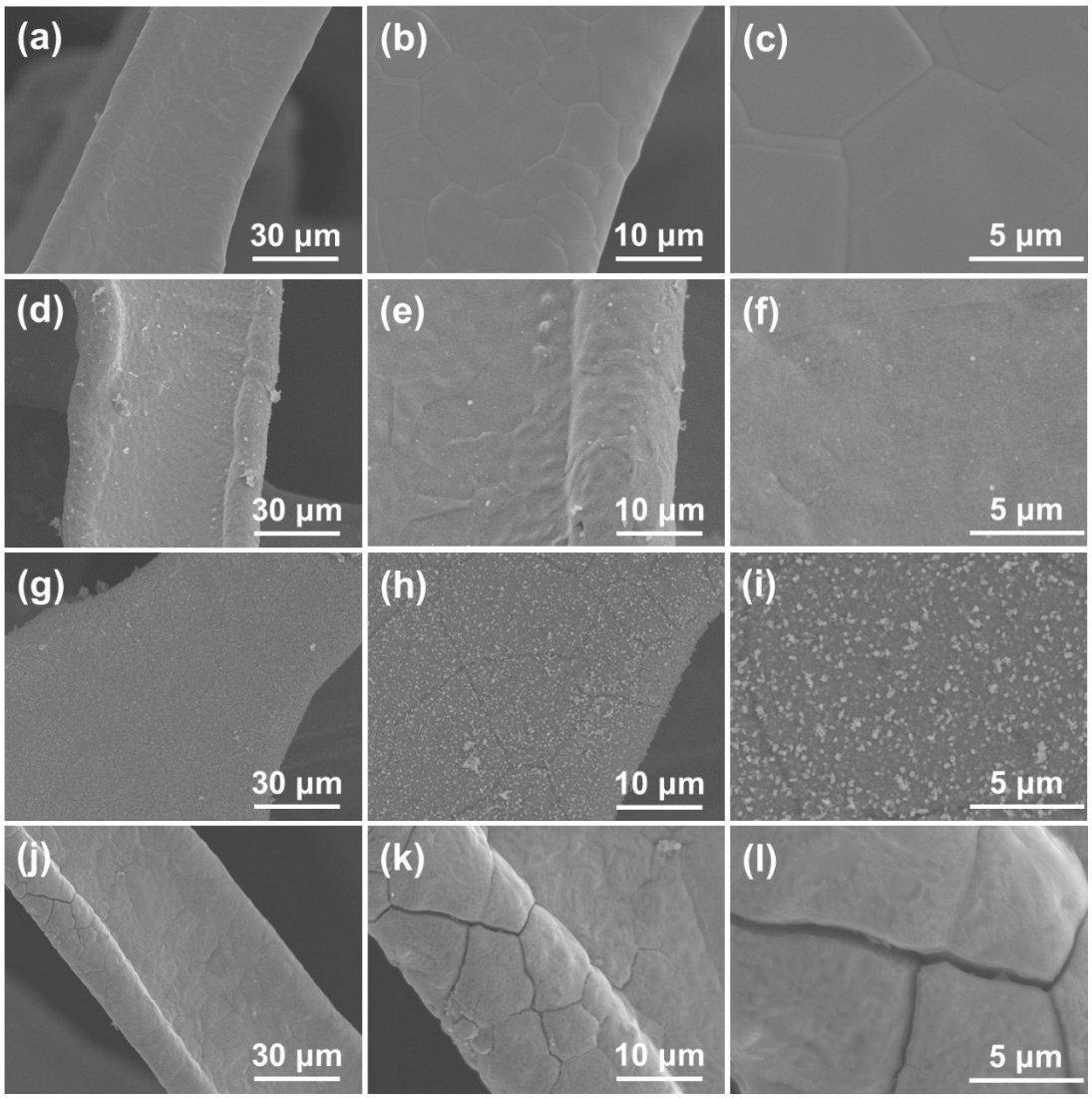

Fig. S1. SEM images of (a-c) NF, (d-f) precursor, (g-i) NF@Sn/C and (j-l) NF@C at different magnifications.

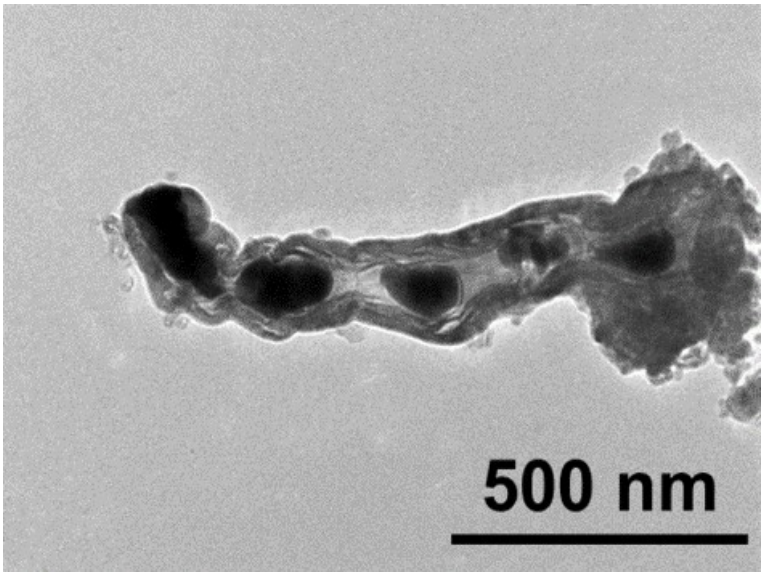

Fig. S2. TEM image of DLCTs with the bamboo-like structure and visible Sn particles.

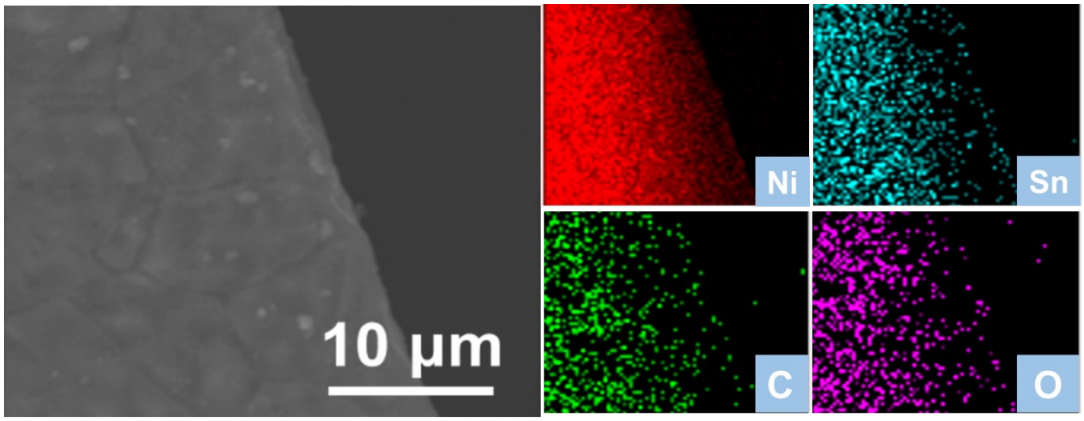

Fig. S3. Elemental mapping images of the precursor. It can be clearly observed that there are homogeneous distributions of Ni, Sn, C and O elements in the precursor.

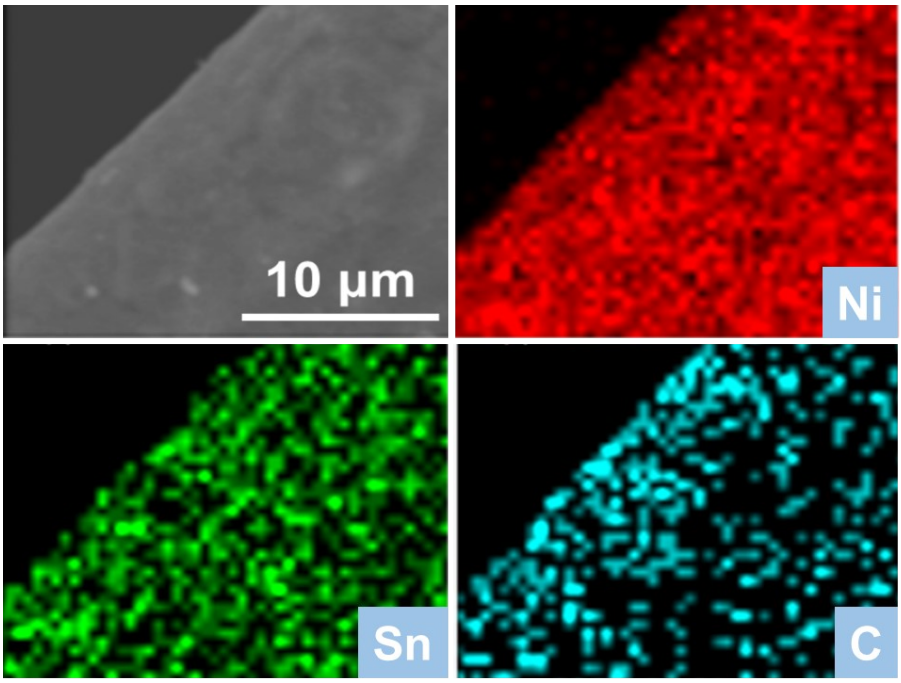

Fig. S4. Elemental mapping images of the as-prepared NF@Sn/C. Specially, there are homogeneous distributions of Ni, Sn and C elements in the as-prepared NF@Sn/C.

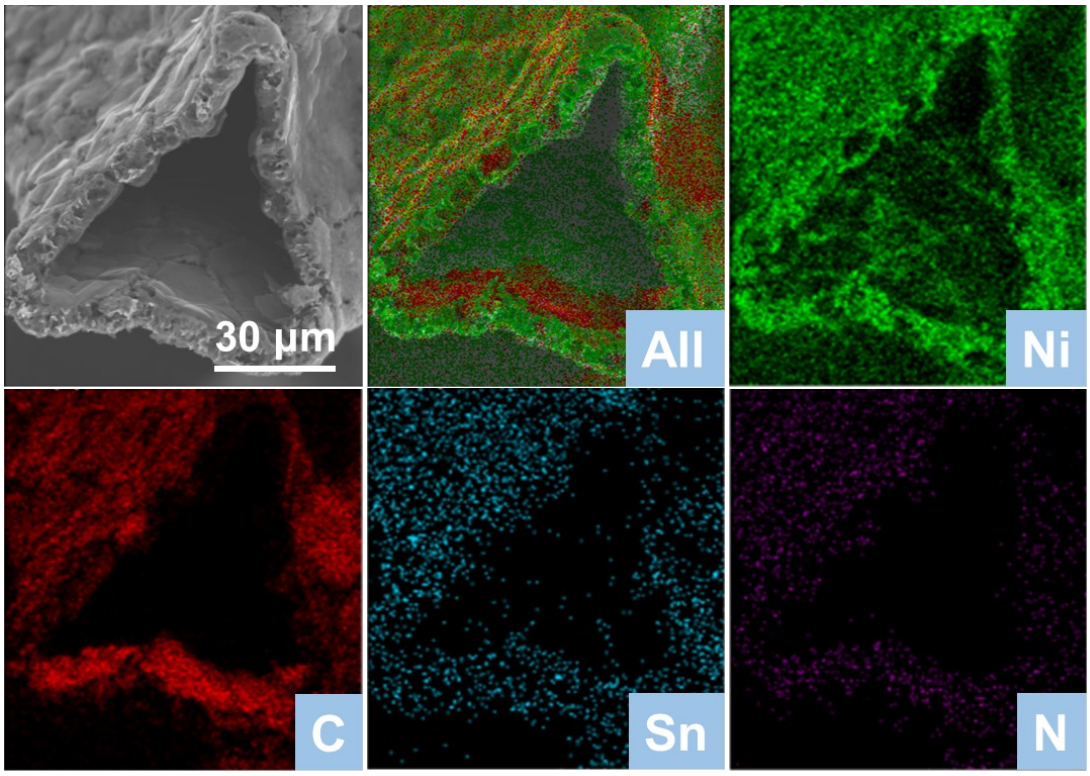

Fig. S5. Cross-section elemental mapping images of the as-prepared DLCTs. It reveals that the Sn-containing and N-doped carbon tubes covered uniformly on the NF surface in the as-prepared DLCTs.

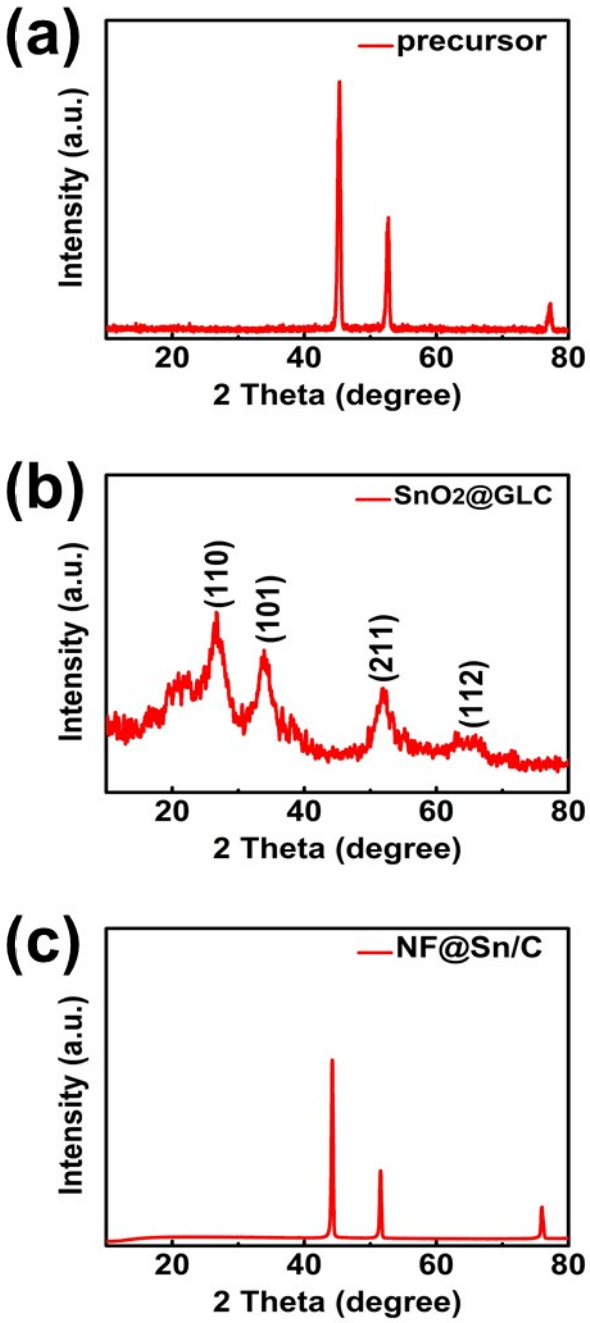

Fig. S6. XRD patterns of (a) the precursor, (b) SnO_2@GLC and (c) NF@Sn/C. Notably, three obvious peaks located at 45.3°, 52.7° and 77.3° are ascribed to the metallic Ni (**Fig. S6a),** and four peaks located at 26.8°, 33.9°, 51.9° and 64.7° could be attributed to SnO_2 (**Fig. S6b**).

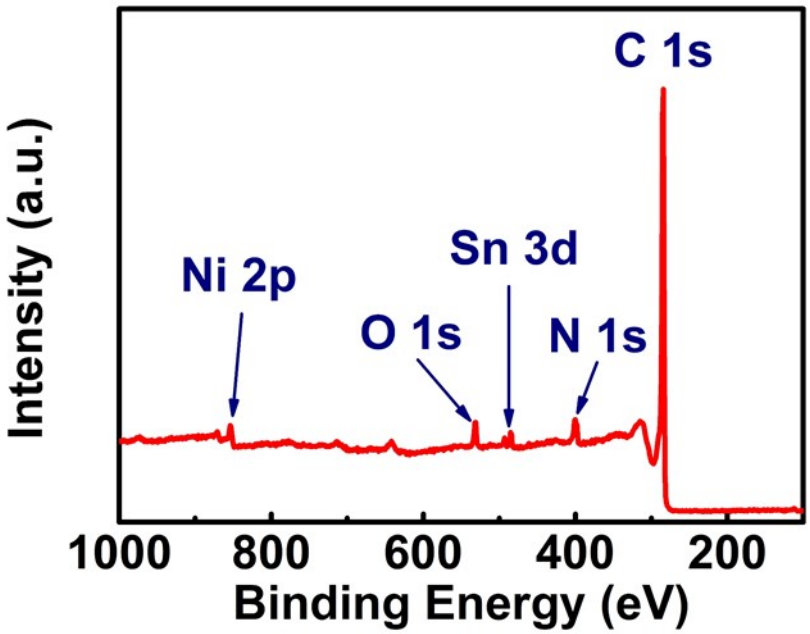

Fig. S7. XPS spectra of the DLCTs. There are five types of elements to investigate the surface characterization in the XPS spectra, namely C, Ni, Sn, N, and O respectively.

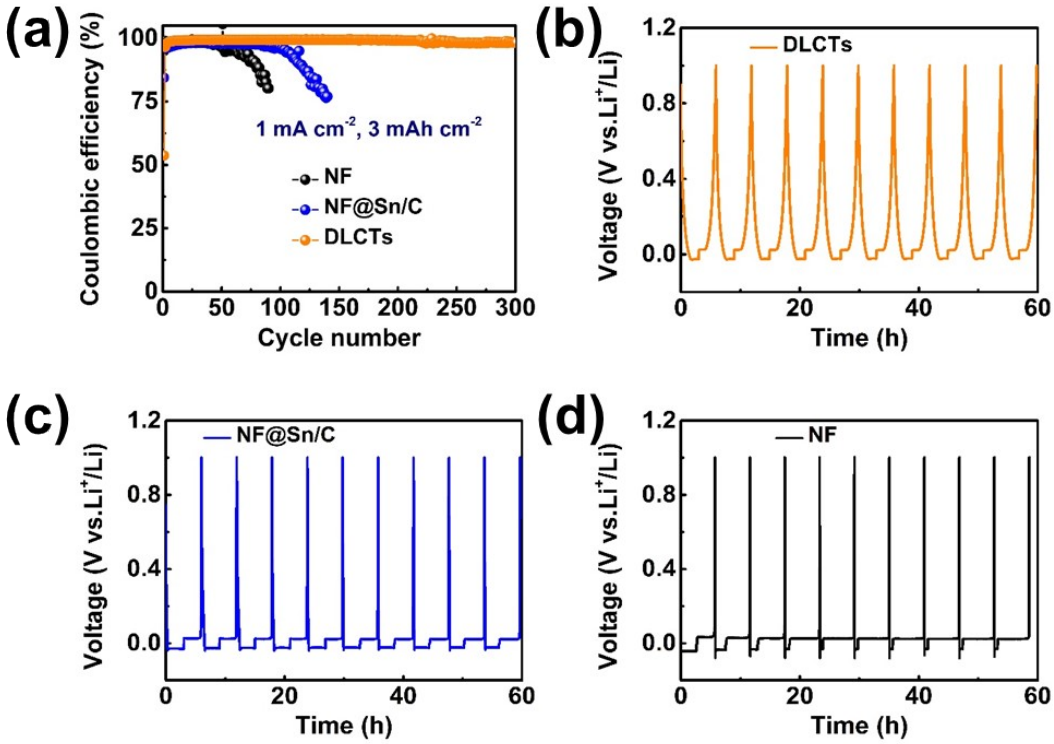

Fig. S8. (a) Coulombic efficiency profiles of NF, NF@Sn/C and DLCTs at a fixed current density of 1 mA cm^{-2} with an areal capacity of 3 mAh cm^{-2}, and the corresponding voltage-time profiles of (b) DLCTs, (c) NF@Sn/C and (d) NF.

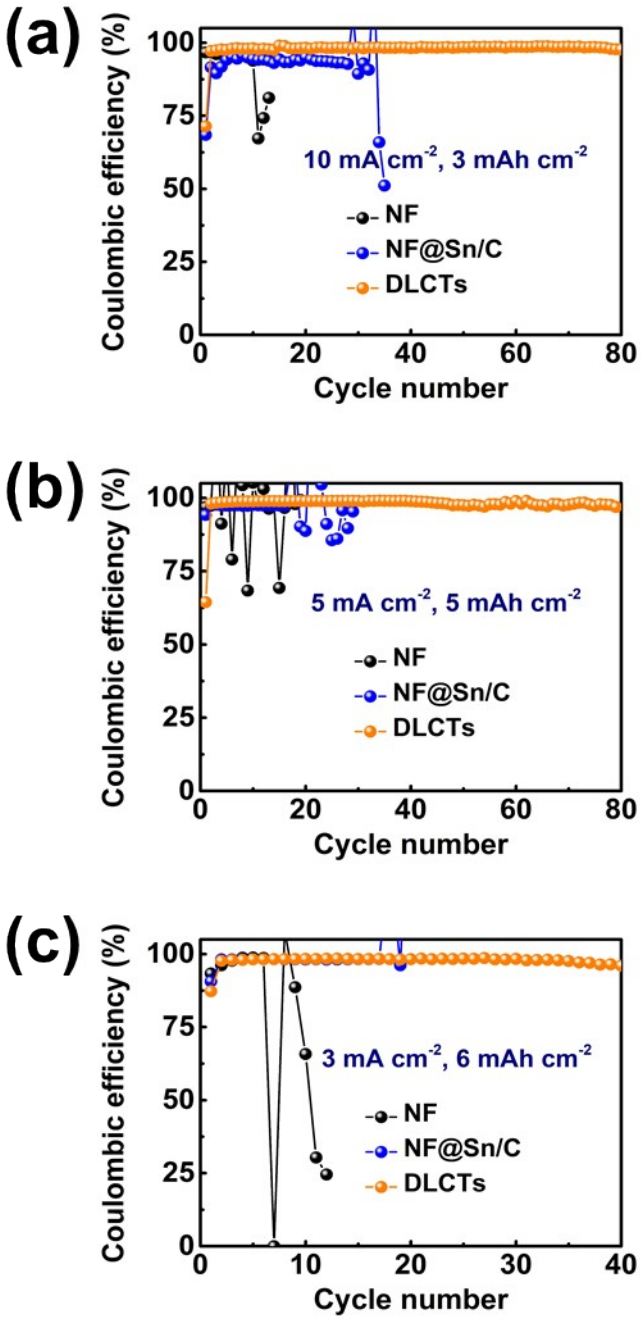

Fig. S9. Coulombic efficiencies of NF, NF@Sn/C and DLCTs: (a) 10 mA cm^{-2} with 3 mAh cm^{-2}, (b) 5 mA cm^{-2} with 5 mAh cm^{-2} and (c) 3 mA cm^{-2} with 6 mAh cm^{-2}.

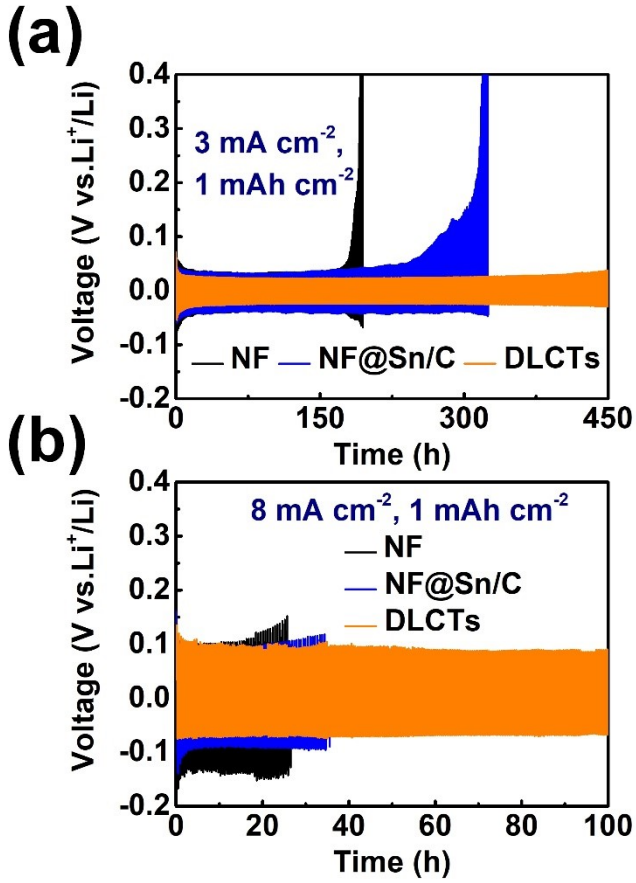

Fig. S10. Voltage-time profiles of NF, NF@Sn/C and DLCTs: (a) 3 mA cm^{-2} with 1 mAh cm^{-2} and (b) 8 mA cm^{-2} with 1 mAh cm^{-2}.

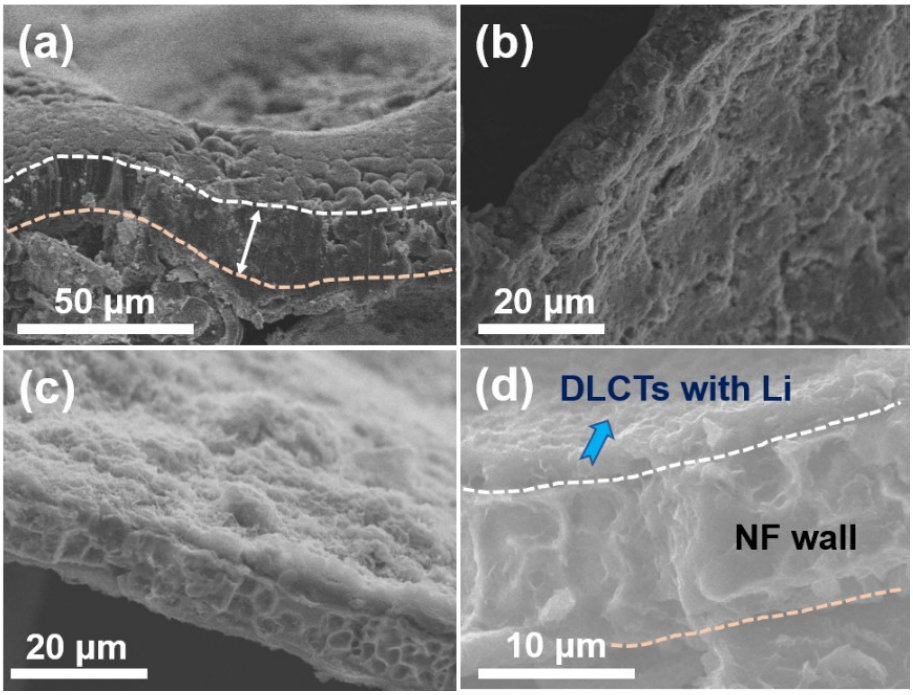

Fig. S11. (a) SEM images of DLCTs loaded with the Li metal of 10 mAh cm^{-2}. SEM images of DLCTs@Li electrode after (b) 25 and (c-d) 50 cycles at 5 mA cm^{-2} with 5 mAh cm^{-2}.

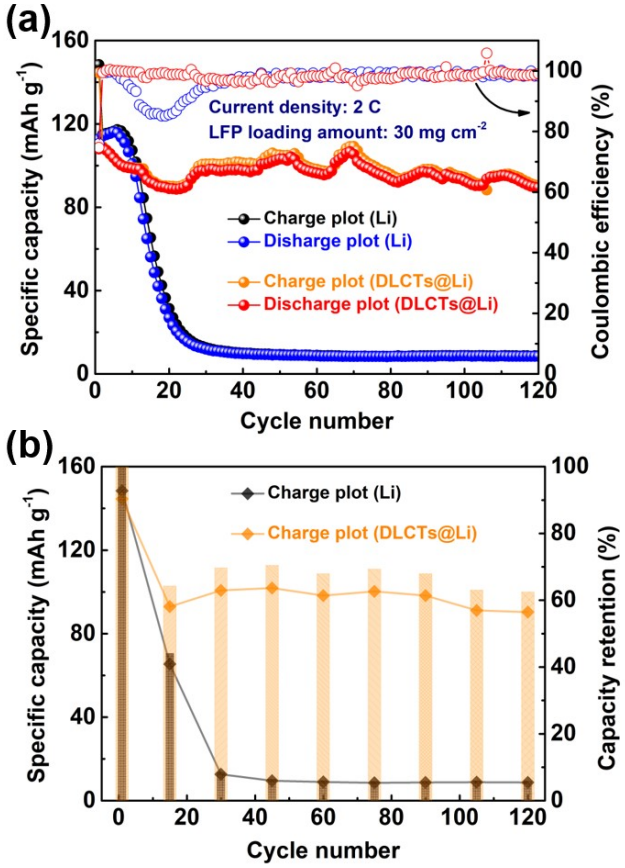

Fig. S12. (a) Electrochemical performances of full cells with high $LiFePO_4$ loading of 30 mg cm^{-2} at the current density of 2 C. (b) Related plots of specific capacity and capacity retention at various cycles.

Table S1 Electrochemical properties comparison of DLCTs and relative three-dimensional porous frameworks obtained by modifying Ni foam (NF) or Cu foam (CF).

Materials	Current density	Areal capacity	Lifetime (h)	Ref.
Li-Zn@CF	1 mA cm^{-2}	1 mAh cm^{-2}	430	1
LNCO/Ni	1 mA cm^{-2}	1 mAh cm^{-2}	1000	2
NCNT/NF	1 mA cm^{-2}	1 mAh cm^{-2}	1000	3
CNF@NF	1 mA cm^{-2}	1 mAh cm^{-2}	300	4
Au/Cu@FCu	1 mA cm^{-2}	1 mAh cm^{-2}	970	5
ZMNF	2 mA cm^{-2}	2 mAh cm^{-2}	800	6
CONF	2 mA cm^{-2}	2 mAh cm^{-2}	167	7
NiO@NF	1 mA cm^{-2}	1 mAh cm^{-2}	600	8
$AuLi_3$@NF	0.5 mA cm^{-2}	1 mAh cm^{-2}	740	9
This work	**2 mA cm^{-2}**	**2 mAh cm^{-2}**	**1200**	
	5 mA cm^{-2}	**5 mAh cm^{-2}**	**200**	

References for Table S1

1 Y. Ye, Y. T. Liu, J. L. Wu, Y. F. Yang, *J. Power Sources*, 2020, **472**, 228520.

2 X. Huang, X. Y. Feng, B. Zhang, L. Zhang, S. C. Zhang, B. Gao, P. K. Chu, K. F. Huo, *ACS Appl. Mater. Interfaces*, 2019, **11**, 31824-31831.

3 Z. Zhang, J. L. Wang, X. F. Yan, S. L. Zhang, W. T. Yang, Z. H. Zhuang, W. Q. Han, *Energy Storage Mater.*, 2020, **29**, 332-340.

4 Z. P. Zeng, W. Li, X. J. Chen, X. B. Liu, *Adv. Funct. Mater.*, 2020, **30**, 2004650.

5 N. Luo, G. J. Ji, H. F. Wang, F. Li, Q. C. Liu, J. J. Xu, *ACS Nano*, 2020, **14**, 3281-3289.

6 C. Z. Sun, Y. P. Li, J. Jin, J. H. Yang, Z. Y. Wen, *J. Mater. Chem. A*, 2019, **7**, 7752-7759.

7 X. Y. Yue, W. W. Wang, Q. C. Wang, J. K. Meng, Z. Q. Zhang, X. J. Wu, X. Q. Yang, Y. N. Zhou, *Energy Storage Mater.*, 2018, **14**, 335-344.

8 Y. Ma, Y. X. Jing, Y. T. Gu, P. W. Qi, Y. B. Lian, C. Yang, A. A. Razzaq, X. H. Zhao, Y. Peng, X. Q. Zeng, J. S. Li, Z. Deng, *ACS Appl. Mater. Interfaces*, 2020, **12**, 9355-9364.

9 X. Ke, Y. H. Liang, L. H. Ou, H. D. Liu, Y. M. Chen, W. L. Wu, Y. F. Cheng, Z. P. Guo, Y. Q. Lai, P. Liu, Z. Shi, *Energy Storage Mater.*, 2019, **23**, 547-555.